Potential Effects of Climate Change on Winter Turbidity Levels in the Ashokan Reservoir, NY

NIHAR R. SAMAL,[1] ADAO. H. MATONSE,[1] RAJITH MUKUNDAN,[1] DONALD C. PIERSON,[2] RAKESH K. GELDA,[3] MARK S. ZION,[2] AND ELLIOT M. SCHNEIDERMAN[2]

ABSTRACT

Transport of high concentrations of suspended particles is one of the major water quality concerns for water supply reservoirs, including the New York City water supply system (NYCWSS). Ongoing changes in snowpack accumulation and winter streamflow patterns could potentially lead to increased turbidity levels in early winter and a reduction in turbidity loads at the time of traditional spring runoff. In this study we examine the potential effects of these simulated changes on reservoir turbidity levels. Our analysis focuses on Ashokan Reservoir, which can at times receive significant watershed turbidity inputs mainly from stream channel erosion from the Esopus Creek. Both measured and simulated turbidity loads and climatology are input to CE-QUAL-W2 (W2), a reservoir turbidity transport model that can simulate reservoir turbidity and other water quality parameters. In this study, the W2 model is applied to estimate the effects of hydro-climatology on settling rates and turbidity transport as a result of differences in reservoir thermal structure during summer and winter events. Our results indicate that the two-dimensional hydrodynamic transport model is able to capture summer and winter turbidity processes. Simulations suggest that the settling velocity is substantially lower at low temperatures during winter time. Winter average stream flow is simulated to increase by 12 and 20%, which lead to increases in reservoir turbidity by 11 and 17% for the future period 2046–2065 and 2081–2100, respectively. This analysis is expected to have potential implications for reservoir operations under winter conditions.

Keywords: stream turbidity, reservoir turbidity, W2 model; climate change, winter settling rate, snowmelt runoff.

INTRODUCTION

Intermittent inflows of high concentrations of suspended particles to Catskill system reservoirs is one of the water quality concerns affecting the New York City water supply system (NYCWSS). Turbid water in a reservoir has negative aesthetic and recreational appeal. Mitigating the impacts of high turbidity may require changes in reservoir operations, which may increase water delivery and treatment costs. Following high streamflow events when high loads of inorganic particles are transported, elevated turbidity (T_n, NTU) levels with complex spatial

[1] Institute for Sustainable Cities, City University of New York, NY 10065, USA. Corresponding author: Nihar Samal, Research Associate, City University of New York and Deptartment of Civil Engineering, National Institute of Technology Durgapur, M.G. Avenue, West Bengal, INDIA; nsamal@hunter.cuny.edu.
[2] New York City Department of Environmental Protection, Kingston, NY 12401, USA.
[3] Upstate Freshwater Institutes, Syracuse, NY 13204, USA.

pattern in downstream lakes and reservoirs can occur (Effler et al., 2006; Gelda and Effler, 2007; Prestigiacomo et al., 2008; Gelda et al., 2012). Distribution and transportation of these particles in lakes and reservoirs are time and space varying (Casamitjana and Schladow, 1993) and are further influenced by the hydro-meteorological forcings. Changes in meteorological forcings can lead to changes in reservoir thermal stratification resulting in changes in the distribution of turbidity. In the unstratified winter period, a reservoir is well mixed; and high turbidity levels may be observed due to winter storm events (Lou and Schwab, 2000).

Various studies have been undertaken on particle size, particle distribution, and transport processes (Casamitjana and Schladow, 1993; MacIntyre et al., 1999; Brach-Papa et al., 2006; Bilotta and Brazier, 2008; Chakraborti et al., 2009; Chung et al., 2009; Gelda et al., 2009, 2012); but specific mechanisms concerning temperature effects on particle transport following large and small events in a large reservoir system have not been thoroughly addressed, especially effects that would occur during low temperatures and isothermal conditions. The seasonality of streamflow and particle transport may vary under future climate due to changes in winter snowmelt and shifts in seasonality of streamflow in the northeastern region of the US (Mukundan et al., 2012; Matonse et al., 2012, 2011). In context of the seasonal variability in streamflow and associated changes in stream turbidity, this investigation is made to document the effects of summer and winter turbidity inputs to the Ashokan reservoir and to assess the turbidity and temperature distributions in the reservoir prior to and after several summer and winter turbidity inputs. The effects of temperature on settling rate in the reservoir following summer and winter events and the potential impact of climate change on future turbidity level in reservoir are examined.

Historical simulations

The fate and transport of turbidity loads entering the Ashokan Reservoir is determined using W2 model (Cole and Buchak, 1995; Cole and Wells, 2002), which has been adapted, calibrated, and rigorously tested for the Ashokan Reservoir (Gelda et al., 1998, 2009). The simulations presented here are for the West Basin of Ashokan Reservor, which is represented in the model by a grid of cells with 28 longitudinal segments and vertical layers of 1 m thickness (Figure 1). The driving data for the model under historical conditions (1948–2011) include measured time series of daily reservoir inflows with associated stream temperature (T) and turbidity T_n; meteorological data (hourly air temperature, dew point, solar radiation, wind speed, and wind direction); and daily records of operational information (withdrawal, spill and release volumes, and reservoir water surface elevation).

Model results for in-reservoir water temperature and turbidity for more recent years (2006–2011) were compared with data collected at automated profile buoys located within the reservoir. The two buoys were located at sites about midway longitudinally from the Esopus Creek inflow to the dam (site 1.4) and near the dam (site 3.1). We presented the buoy measurements near the dam (buoy 3.1) for calibration. Data are collected four times a day (6 hour increments) and include water temperature and turbidity measured from the surface to the bottom of the reservoir at 1 m depth increments (Gelda et al., 2009). Event-based sampling is also conducted in order to support our modeling study.

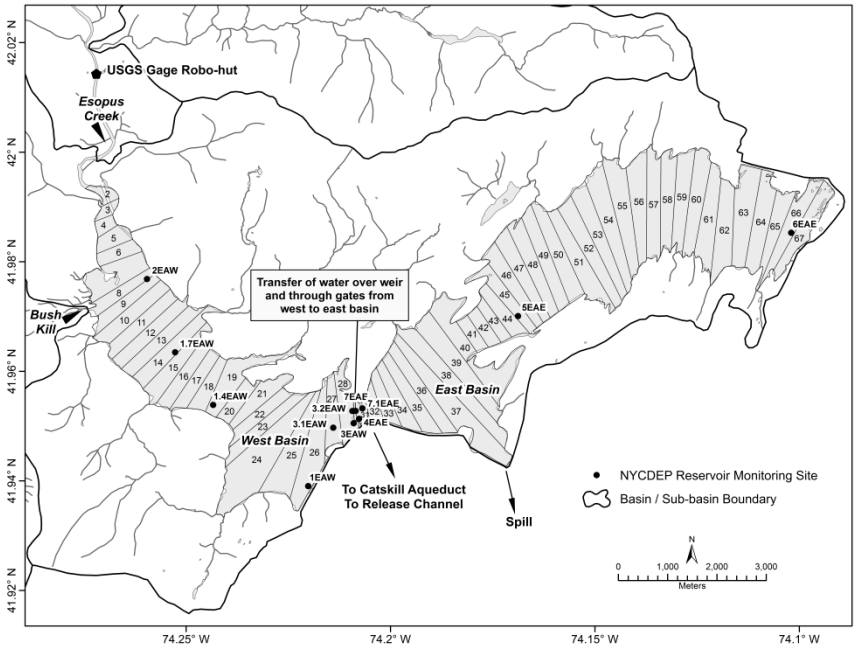

Figure 1. Ashokan Reservoir (West and East Basin): mouth of Esopus Creek and Bush Kill with model segment identification number

Future climate scenarios

Climate scenarios were developed from the output of three GCMs: CGCM3.1, CNRM-CM3, and MRI-CGCM2.3.2. Table 1 summarizes the climate scenarios and time periods used in this study. Scenarios of daily air temperature and precipitation were created by downscaling the different GCMs (Anandhi et al., 2011) and scenarios for the region of study using a 25-bin change factor methodology. Change factors created by this method were applied to historical records of daily meteorological data to develop local future climate scenarios.

Table 1. General Circulation Models, emission scenarios and time slices applied in this study.

GCM	Emission scenario	Time Slices
GCMs: CGCM3.1 (Canada)	A1B, A2, B1	2081–2100
	B1	2046–2065
CNRM-CM3 (France)	B1	2046–2065, 2081–2100
MRI-CGCM2.3.2 (Japan)	B1	2081–2100

For reservoir model application hourly meteorological future climate scenarios were created from the daily climate scenarios. Hourly air temperature was estimated using future simulated daily minimum (Tmin) and maximum (Tmax) air temperatures and the WAVE model as described in Reicosky et al. (1989). The WAVE model uses today's Tmin and Tmax together with next day Tmin to compute hourly air temperature from today's sunrise (*Rise*) to 1400h and from 1400h to sunrise of the next day. Hourly temperature (*T(H)*) is estimated as

$$T(H) = Tave + Amp(\cos(\pi H' / Rise))) \quad (1)$$

for $0 \leq H < Rise$ and $1400h < H \leq 2400h$ and

$$T(H) = Tave - Amp(\cos(\pi(H - Rise)/(14 - Rise))) \quad (2)$$

for $Rise \le H \le 1400h$; where

H is the time in hours
$H' = H + 10$ if $H < Rise$
$H' = H - 14$ if $H > 1400h$
$Tave = (Tmin + Tmax)/2$
$Amp = (Tmax - Tmin)/2$.

In absence of future sunrise data, we used historical regional daily sunrise times.

The dew point temperature for W2 climate change simulations is set equal to simulated hourly *Tmin*, and future wind and solar radiation are set equal to local historical hourly values.

Climate change inflows to the West Basin Ashokan Reservoir are simulated on a daily time step using the Generalized Watershed Loading Functions-Variable Source Area (GWLF-VSA) model (Schneiderman et al., 2007; Schneiderman et al., 2002; Haith and Shoemaker, 1987). The GWLF-VSA model was calibrated using historical inputs to simulate streamflow from Esopus Creek at Coldbrook and Bush Kill, which contribute to West Basin Ashokan Reservoir inflow. In addition, inflow from ungauged areas draining to the reservoir is estimated using Bush Kill estimates and a ratio between Bush Kill and ungauged drainage areas. A rating curve (Gannett Fleming and Hazen and Sawyer, 2008), developed empirically using historical data, is used to estimate turbidity concentration T_n based on simulated Esopus Creek flow Q_{Esp} and has the form

$$\log T_n = 1.033 - 0.986 \log Q_{Esp} + 0.691(\log Q_{Esp})^2 \quad (3)$$

A lower bound $T_n = 4.8$ is used for $Q_{Esp} < 5.17$ m^3/s. Total daily turbidity is then partitioned into three particle sizes using the following criteria:

$T_{n1} = 0.10 \times T_n$ (4a)

If $Q_{Esp} > 40$ m^3/s, $T_{n2} = 0.45 \times T_n$,
and $T_{n3} = 0.45 \times T_n$; else $T_{n2} = 0.65 \times T_n$ and $T_{n3} = 0.25 \times T_n$. (4b)

Future values of Esopus Creek water temperature at hour i (T_i) is calculated in °C using the following regression equation developed by the Upstate Freshwater Institute (UFI) and published in NYC DEP (2007):

$$T_i = a_0 + a_1 \times T_{air,i-2} + a_2 \times \log Q_{Esp} + a_3 \times a_5 \times T_{STP,i}^{a_4} \quad (5)$$

where

T_{air-2} is the simulated local air temperature of two hours back (in °C)
a_0–a_5 are the model coefficients calibrated on a monthly basis using historical data
Q_{Esp} is the simulated Esopus Creek daily average streamflow in cubic meters per second (m^3/s)
$T_{STP,i}$ is the Shandaken tunnel portal temperature at the ith hour
Coefficient a_5 is 0 when the Shandaken tunnel is off and 1 when the tunnel is on.

As part of the NYC water supply operations, water from the nearby Schoharie reservoir can be routed through Shandaken Tunnel to the Esopus Creek that flows into the Ashokan Reservoir. When running future climate scenarios, these and other operational flows are obtained from the NYC OASIS model (Operational Analysis and Simulation of Integrated Systems, HydroLogics,

Inc., 2007) simulations using similar climate change inflows. For the West Basin Ashokan Reservoir these include the Shandaken Tunnel flows, the gate flows in the dividing weir between the West and East Basins of the Ashokan Reservoir, and the release channel withdrawals from West Basin Ashokan. The time series for these flows are obtained from OASIS on a daily time step.

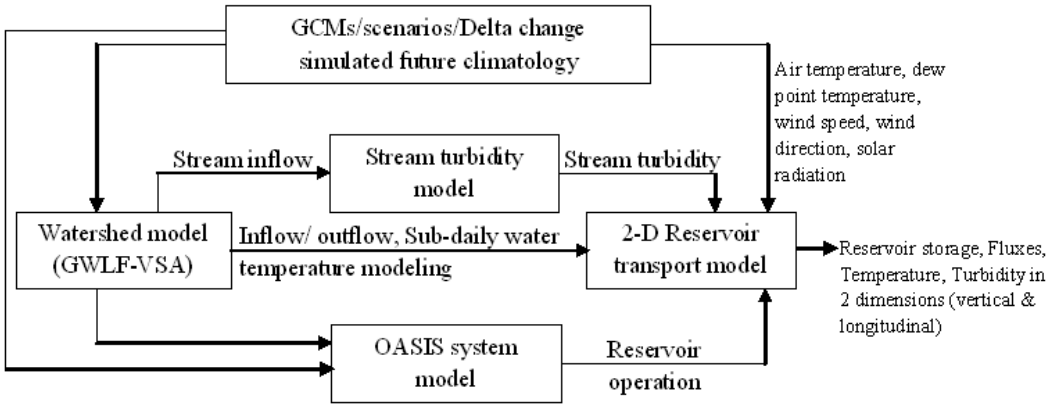

Figure 2. Modeling frame work: Model connection and data flow

Figure 2 illustrates the modeling framework applied for this study. Inputs to the W2 model include downscaled GCM/Scenarios climate data, simulated hourly climate developed using various methods based on simulated daily hydrology and climatology, watershed model simulated daily streamflow, daily stream turbidity simulated using a turbidity model that uses simulated streamflow, and daily reservoir operations simulated by the OASIS (Hydrologics, Inc., 2007) reservoir system model.

RESULTS AND DISCUSSIONS

Evaluation of W2 model performance using historical data

The W2 model was previously calibrated and validated for the Ashokan reservoir using volume weighted epilimnetic and hypolimnetic temperature as described in Gelda et al. (2009). For further testing, the model was driven with the actual observed streamflow and stream turbidity for the period 2003 to 2011 and evaluated by comparing model versus observed data of (1) reservoir water surface elevations (June 2003 to September 2011) (Figure 3) and (2) reservoir turbidity measured at robotic monitoring site 3.1 for 2006 to 2011 (Figure 4).

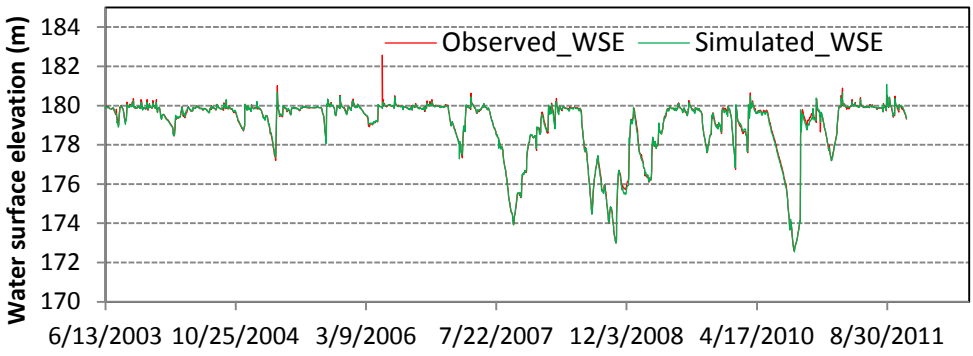

Figure 3. Model simulated and observed water surface elevations in Ashokan Reservoir for the period 2003–2011

The model simulates well the fluctuations in water surface elevations both during low and high flow event period except for 11 May 2006 (Figure 3). The three drops in water surface elevations below 174 m are observed on 23 September 2007, 19 October 2008, and 04 September 2010 and are well represented by the model simulation. Sharp rises in water surface elevations correspond to large storm event inputs of water to the reservoir.

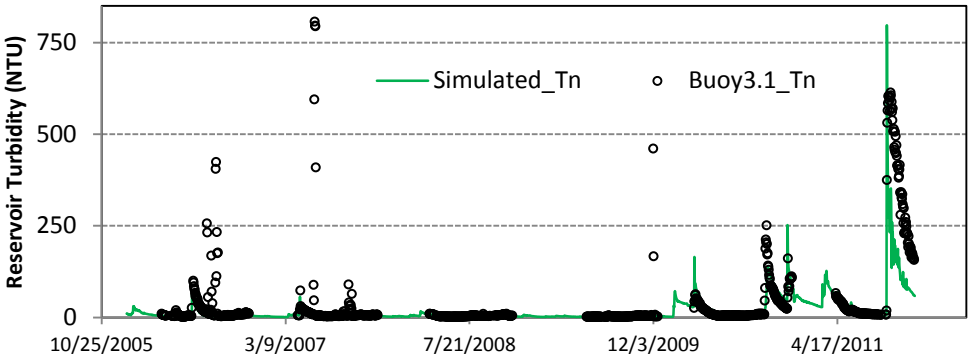

Figure 4. Model versus observed turbidity (T_n, NTU) in Ashokan Reservoir, 2006–2011, where the green line represent the model turbidity at segment 28 (Withdrawal point)

Figure 4 illustrates how the model simulated reservoir turbidity compares to observed data at buoys 3.1 of the West Basin available for the period 2006–2011. The model simulated turbidity levels are similar to the buoy measured data in all cases except in case of a few high outlying measurements late October and early November. While it is impossible to state the source of these errors, the intermittently high measured data suggests the problem is more likely with the buoy measurements

Event sampling from simulated time series

To evaluate and better understand the seasonal pattern between streamflow, stream turbidity, and reservoir turbidity, we sampled the historical model results for two seasons, summer (May–October) and winter (November–April), during more than six decades of historical record (1948–2011). A total of 12 events considering a wide range of streamflows were examined (Table 2). when choosing these events, an average daily streamflow of 146 m^3/s was selected as minimum

streamflow that caused the average reservoir turbidity to rise above 10 NTU. Figure 4 Illustrates summer and winter turbidity response using data from two different storm events.

Table 2. Same size paired events during summer and winter.

Summer				Winter			
Date of peak streamflow	Stream-flow (m^3/s)	Peak stream turbidity (NTU)	Peak reservoir turbidity (NTU) *	Date of peak streamflow	Stream-flow (m^3/s)	Peak stream turbidity (NTU)	Peak reservoir turbidity (NTU) *
09-07-1999	191	228	12	11-28-1993	233	283	83
09-18-2004	250	15	12	12-08-1974	240	306	58
10-21-1995	254	351	28	12-2-1996	271	413	92
06-28-2006	322	468	68	11-08-1977	304	557	95
06-28-2006	322	468	68	03-23-2010	350	595	165
10-01-2010	500	1440	138	04-03-2005	500	315	69

* turbidity at segment 28

Summer: Winter:

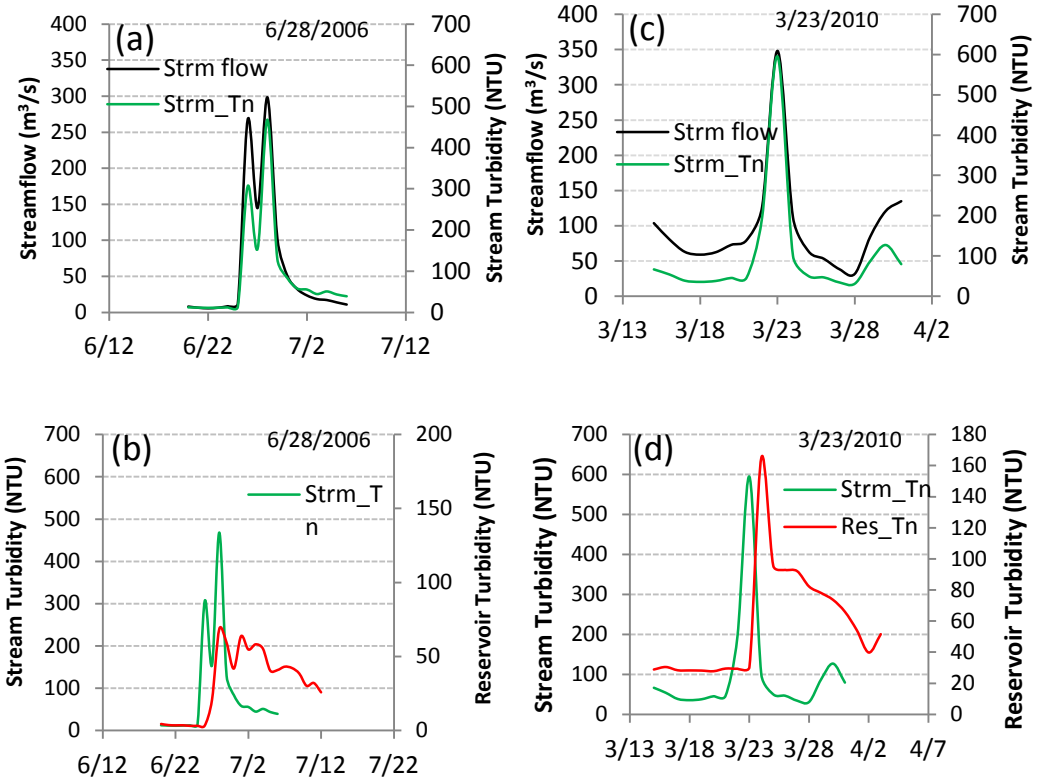

Figure 5. Similar size paired summer and winter event; the reservoir turbidity is at segment 28 (withdrawal point).

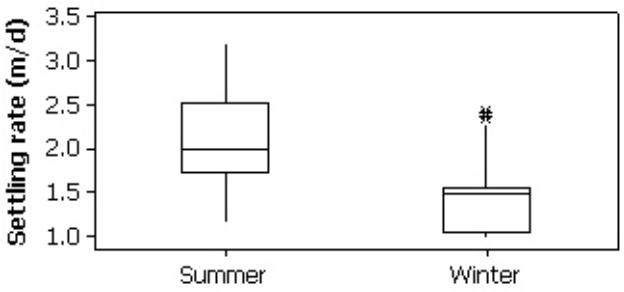

Figure 6. Summer and winter settling velocities based on Stoke's Law.

For similar streamflow size events, the reservoir turbidity was found to be higher in the winter compared to summer, as illustrated by the examples in Figure 5. These results can be explained given the fact that higher temperatures in summer lead to faster settling rates and resulted in lower turbidity (Figure 6). High turbidity events tend to be more frequent during winter. Because of the winter isothermal condition, the turbidity plumes have a longer travel time in the reservoir resulting in overlapping effects between consecutive turbidity events.

Event specific temperature-turbidity profiles in Ashokan reservoir

Simulated reservoir water temperature and turbidity profiles during summer and winter events are shown in Figure 7 and 8. The reservoir temperature is stratified before the occurrence of an event during summer (Figure 7a) and near isothermal during winter (Figure 8a). During the summer event, warmer epilimnetic temperature forms an upper mixed layer; and the wind induced turbulence energy is not sufficient to establish an isothermal water column (Figure 7a). The warmer epilimnetic temperatures in part reflect higher ambient air temperature during the summer event period. For these two events, the summer and winter streamflow events are of similar size (Figure 5a), but summer event turbidity is found to be higher in upper few meters (5–10 m) and lower (< 5 NTU) below the upper mixed layer (Figure 7b). This behavior is related to temperature (density) of input stream water matching temperature of epilimnion and turbidity being concentrated above thermocline and being transported as a plume due to slow settling of clay particles.

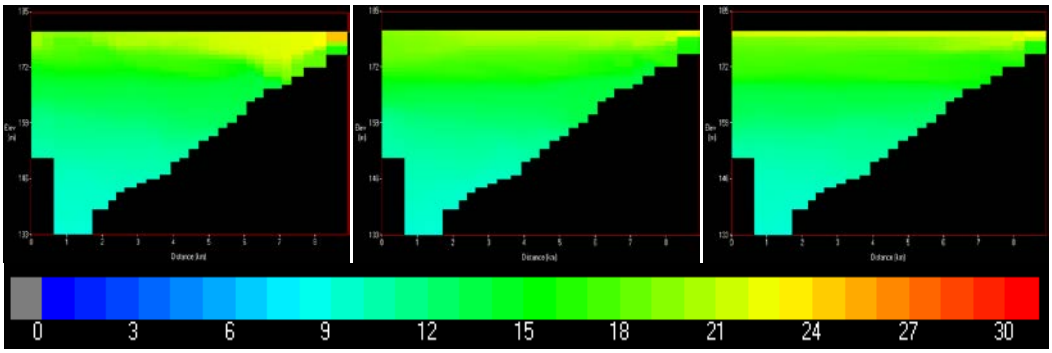

Figure 7a. Temperature distribution before, during and after a summer event (06/28/2006)

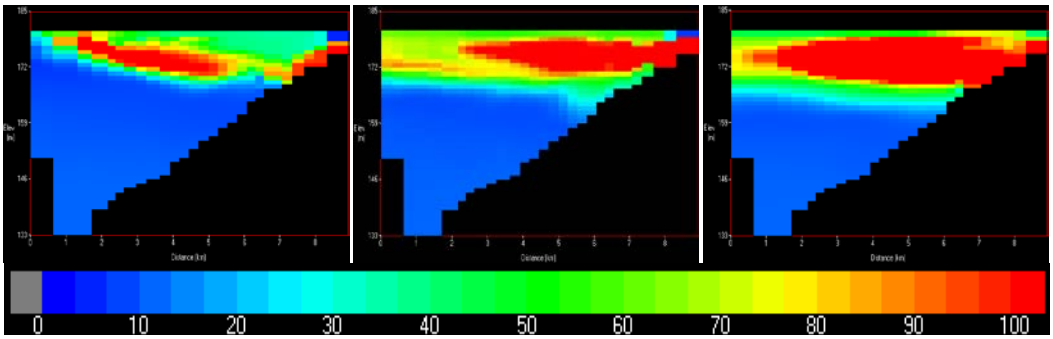

Figure 7b. Turbidity distribution before, during, and after a summer event (06/28/2006). X-axis: Distance (km) from model segment 28 (0 km) to segment 1 (9 km); Y-axis: Elevation (m) from bottom (133 m) with scale factor 13 meter).

Before the winter event (Figure 8), the turbidity appears evenly distributed at about 30–40 NTU throughout the reservoir due to a preceding event. A turbidity plume first appears to be moving from stream mouth (segment 1) to the dividing weir (segment 28).

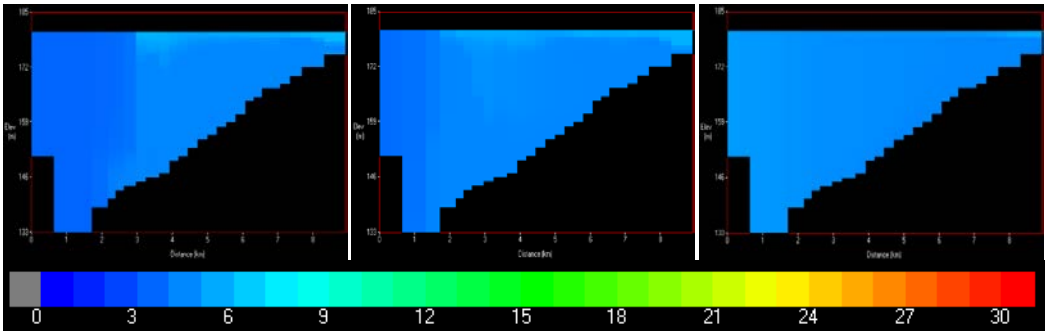

Figure 8a. Temperature distribution before, during, and after a winter event (03/23/2010).

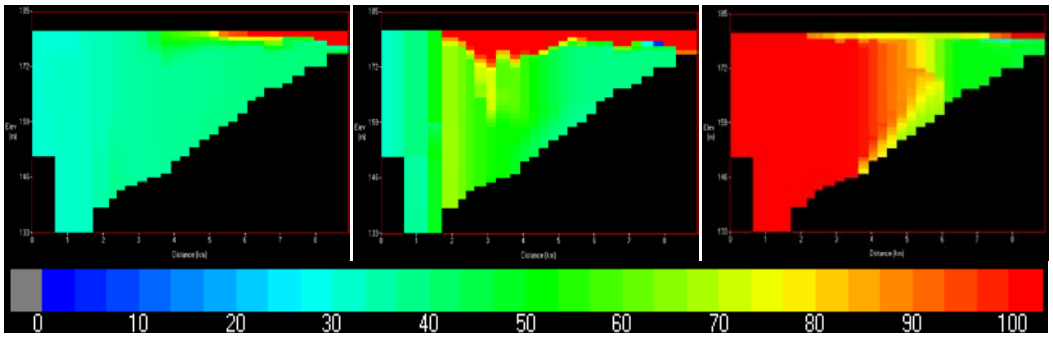

Figure 8b. Turbidity distribution before, during, and after a winter event (03/23/2010). X-axis: Distance (km) from model segment 28 (0 km) to segment 1 (9 km); Y-axis: Elevation (m) from bottom (133 m) with scale factor 13 meter).

The location of the plume may be dependent on the ambient stratification regime and the density of the inflow waters, whereas the magnitude of the peak impact may be a function of the loading. However, the major contrast between the two events (Figure 5 and 7) is related to the thermal structure of the reservoir at the time of the event. In the case of the summer event (Figure 7), the reservoir is stratified; and turbidity moves as a plume above the thermocline. For the winter event (Figure 8), the reservoir is near isothermal; and turbidity is eventually mixed throughout the water column and moves as a plug from upstream to downstream.

Driving parameters and reservoir turbidity under future climate

We have shown how Ashokan Reservoir experiences elevated turbidity levels following summer and winter events. In figure 9 through 12, we compared boxplots representing simulated average monthly future conditions for 2046–2065 (future_4665) and 2081–2100 (future_8100) time periods against baseline conditions for air temperature, streamflow, stream turbidity, reservoir water surface elevation, water temperature, reservoir turbidity and settling velocity. The boxplots represent the 25th (Q1) and 75th (Q3) quartiles (or the interquartile range) from all six climate change scenarios. For both time slices and baseline, the whiskers represent the lowest and highest data values within the lower (Q − 1.5 × (Q3 − Q1)) and upper (Q3 + 1.5 × (Q3 − Q1)) limits. The dark horizontal lines in the box plots represent the median and the asterisks represent outliers.

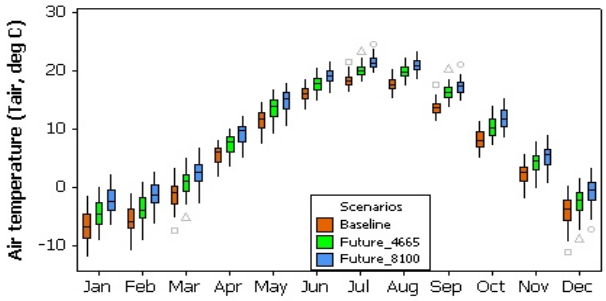

Figure 9. Average monthly air temperature (°C) for the baseline and simulated future period (2046–2065) and 2081–2100.

The air temperature as shown in Figure 9 is projected to increase under future climate conditions with the difference from the baseline being slightly higher for the future_8100 period. The projected average increase in air temperature is +2.0 and +3.5 by future_4665 and future_8100, respectively. The summer and winter season average annual air temperatures is projected to increase by +2.1 and +1.8 by future_4665, whereas it is +3.3 and +3.7 by future_8100 periods. These values are consistent with seasonal trends in historical temperature where average increases in winter temperature are slightly higher than during summer (Hayhoe et al., 2007; Matonse et al., 2011). The higher winter temperature will lead to a reduction in snowpack and may cause more precipitation to fall as rain (Matonse et al. 2012). As a result of changes in snow and precipitation, early winter streamflow is projected to increase (Figure 10a) under future climate scenarios. The streamflow is projected to decrease during March and April and to show minor changes in the following months till October. A similar seasonal pattern is projected for stream turbidity (Figure 10b).

(a) (b)

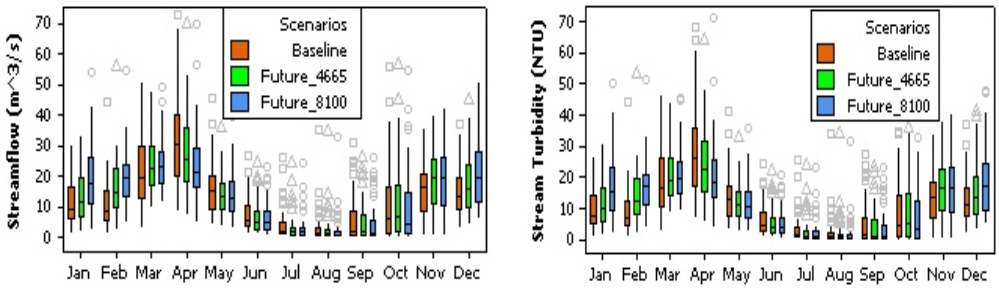

Figure 10 (a) Average monthly inflow (m^3/s); (b) Average monthly Stream Turbidity (T_n, NTU) for the baseline and simulated future period (2046–2065) and 2081–2100.

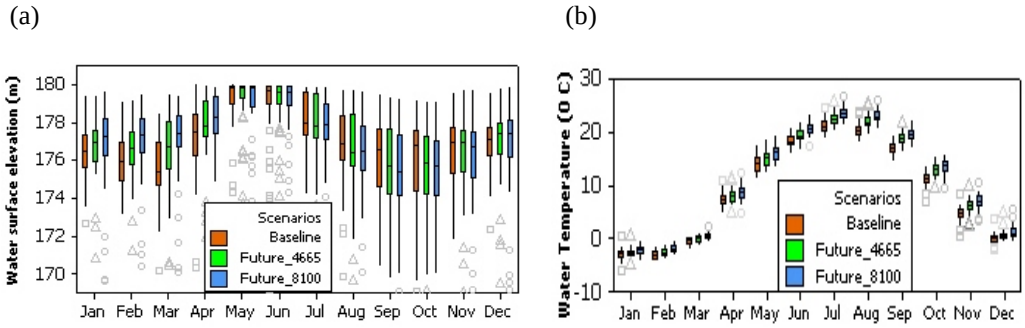

Figure 11. (a) Average monthly water surface elevation (m); (b) Average monthly in-reservoir water temperature (°C) for the baseline and simulated future period 2046–2065 and 2081–2100.

Ashokan Reservoir seasonal water surface elevation (Figure 11a) is simulated to increase during the winter period. The reservoir water temperature (Figure 11b), which is a function of atmospheric forcings and inflows, shows a similar seasonal variation as air temperature (Figure 9). On average, the reservoir water temperature is increased by +1.0 (+1.8), +1.4 (+2.4) during summer and +0.6 (+1.3) during winter by future_4665 (and future_8100) periods. This is an indication of stronger stratification during summer but little change in the largely isothermal conditions during winter. The high winter turbidity and low summer turbidity (Figure 12a) under future climate scenarios are results of increased winter turbidity loading associated with increased future winter stream discharge and also to the variation in winter and summer settling rates (Figure 12b) of turbidity causing particles in the reservoir. The increase in future water temperature influences the mobility of suspended particles and consequently the settling rate.

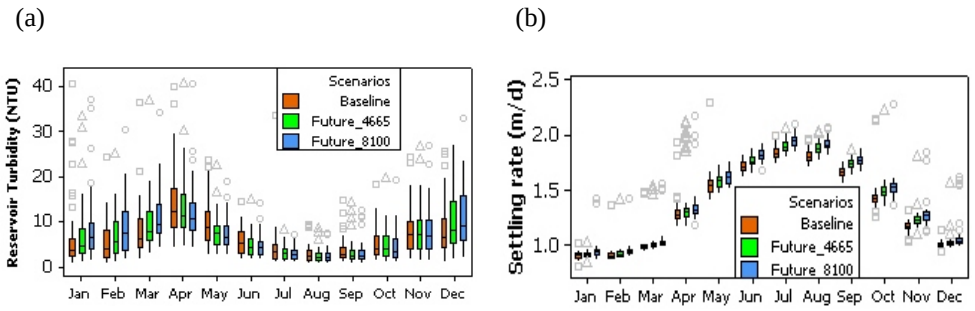

Figure 12. (a) Average monthly reservoir turbidity (T_n, NTU); (b) Average monthly settling velocity (m/day) for the baseline and simulated future period 2046–2065 and 2081–2100.

Under future scenarios, the average annual streamflow is increased by 5 and 7%, which results in an annual increase in reservoir turbidity by 3 and 5% for the future_4665 and future_8100, respectively. However, the average winter reservoir turbidity is increased by 11 and 17% as result of increased in winter stream flow by 12 and 20% for the future_4665 and future_8100, respectively. The climate change scenarios clearly show a shift in timing of streamflow and turbidity loading to the reservoir from a peak in April to earlier in the winter (December–March). This shift in snowmelt driven events causes increased in-reservoir turbidity during December–March, and decreased turbidity in April–May as the peak events of April move to earlier in the year.

CONCLUSIONS

Our results using historical inputs show that the W2 model accurately simulates reservoir water surface elevation and seasonal and event specific reservoir turbidity. As a result of seasonal differences in thermal stratification, the reservoir turbidity generally moves as a plume above the thermocline in summer following a storm event, while in winter, turbidity is generally mixed throughout the water column.

Simulated future reservoir turbidity levels are expected to increase during winter due to earlier snowmelt and resulting shifts in streamflow and turbidity load. Winter isothermal conditions are expected to continue in the future and as a result of relatively low water temperature turbidity settling velocity will remain low.

ACKNOWLEDGEMENTS

The authors are grateful to the New York City Department of Environmental protection (NYCDEP) for providing funding in carrying out this research investigation. Authors acknowledge Ben Wright and Hazen and Sawyer for providing future simulated reservoir operation data. Authors also extend their thanks to David Lounsbury and Donald Kent for their technical support during the preparation of the manuscript.

REFERENCES

Anandhi A, Frei A, Pierson DC, Schneiderman EM, Zion MS, Lounsbury D, Matonse AH. 2011. Examination of change factor methodologies for climate change impact assessment. *Water Resources Research* **47**(3): W03501. DOI:10. 1029/2010WR009104.

Bilotta GS, Brazier RE. 2008. Understanding the influence of suspended solids on water quality and aquatic biota. Water Research **42**(12): 2849–2861.

Brach-Papa C, Boyer P, Ternat F, Amielh M, Anselmet F. 2006. Settling classes for fine suspended particles. *Comptes Rendus Mécanique* **334**(8–9): 560–567.

Casamitjana X, Schladow G.1993. Vertical distribution of particles in stratified lake. *Journal of Environmental Engineering* **119**(3), 443–462.

Chakraborti RK, Atkinson JF, Kaur J. 2009. Effect of mixing on suspended particle-size distribution. *Journal of Environmental Engineering* **135**(5): 306–316.

Chung SW, Hipsey MR, Imberger J. 2009. Modelling the propagation of turbid density inflows into a stratified lake: Daecheong Reservoir, Korea. *Environmental Modelling and Software* **24**(12): 1467–1482.

Cole T, Buchak EM. 1995. *CE-QUAL-W2: A Two-Dimensional, Laterally Averaged, Hydrodynamic and Water Quality Model, Version 2.0*. Instruction Report EL-95-1. US Army Corps of Engineers Waterways Experiment Station: Vicksburg, MS.

Cole TM, Wells SA. 2002. *CE-QUAL-W2: A Two-Dimensional, Laterally Averaged, Hydrodynamic and Water Quality Model, Version 3.1*. Instruction Report EL-02-1. US Army Engineering and Research Development Center: Vicksburg, MS.

Effler SW, Matthews DA, Kaser J, Prestigiacomo AR, Smith DG. 2006. Runoff event impacts on a water supply reservoir: Suspended sediment loading, turbid plume behavior, and sediment deposition. *Journal of the American Water Resources Association* **42**(6), 1697–1710.

Gannett Fleming, Hazen and Sawyer. 2008. *Catskill turbidity control studies: Phase III Implementation Plan.* Prepared for New York City Department of Environmental Protection, Bureau of Engineering Design and Construction.

Gelda RK, Owens EM, Effler SW. 1998. Calibration, verification and an application of a two-dimensional hydrothermal model [CE-QUAL-W2(t)] for Cannonsville Reservoir. *Lake and Reservoir Management* **14**: 186–196.

Gelda RK, Effler SW, Peng F. 2012. Modeling Turbidity and the Effects of Alum Application for a Water Supply Reservoir. *Journal of Environmental Engineering* **138**(1): 38–47.

Gelda RK, Effler SW, Peng F, Owens EM, Pierson DC. 2009. Turbidity model for Ashokan Reservoir, New York: case study. *Journal of Environmental Engineering* **135**(9): 885–895.
Gelda RK, Effler SW. 2007. Modeling turbidity in a water supply reservoir: Advancements and issues. *Journal of Environmental Engineering* **133**: 139–148.
Haith DA, Shoemaker LL. 1987. Generalized watershed loading functions for stream flow nutrients, *Water Resources Bulletin* **23**(3):471–478.
Hayhoe K, Wake CP, Huntington TG, Luo L, Schwartz MD, Sheffield J, Wood E, Anderson B, Bradbury J, DeGaetano A, Troy TJ, Wolfe D. 2007. Past and Future Changes in Climate and Hydrological Indicators in the US Northeast. *Climate Dynamics* 28: 381–407.
Hydrologics Inc. 2007. *User Manual for OASIS with OCL*. Columbia, MD.
Lou J, Schwab DJ. 2000. A model of sediment resuspension and transport dynamics in southern Lake Michigan, *Journal of Geophysical Research* **105**(C3): 6591–6610.
MacIntyre S, Flynn KM, Jellison R, Romero JR. 1999. Boundary mixing and nutrient fluxes in Mono Lake, California. *Limnology Oceanography* **44**(3), 512–529.
Matonse AH, Pierson DC, Frei A, Zion MS, Schneiserman EM, Anandhi A, Mukundan R, Pradhanang SM. 2011. Effects of changes in snow pattern and the timing of run off on NYC water supply system. *Hydrological Processes* **25**: 3278–3288. DOI: 10.1002/hyp.8121.
Matonse AH, Pierson DC, Frei A, Zion MS, Anandhi A, Schneiserman EM, Wright B. 2012. Investigating the impact of climate change on New York City's primary water supply. *Climatic Change* **116**(3–4): 437–456. DOI: 10.1007s10584-012-0515-4.
Mukundan R, Pradhanang SM, Schneiderman EM, Pierson DC, Anandhi A, Zion MS, Matonse AH, Lounsbury DG, Steenhuis TS. 2012. Suspended Sediment Source Areas and Future Climate Impact on Soil Erosion and Sediment Yield in a New York City Water Supply Watershed, USA. *Geomorphology* **183**: 110–119. http://dx.doi.org/10.1016/j.geomorph.2012.06.021.
NYCDEP. 2007. *New York City Water Supply System Reference Guide*. NYCDEP Bureau of Water Supply: Valhalla, New York.
Prestigiacomo AR, Effler SW, O'Donnell DM, Smith DG, Pierson DC. 2008. Turbidity and temperature patterns in a reservoir and its primary tributary from robotic monitoring: Implications for managing the quality of withdrawals. *Lake and Reservoir Management* **24**:231–243.
Reicosky DC, Winkelman LJ, Baker JM, Baker DG. 1989. Accuracy of hourly air temperatures calculated from daily minima and maxima. *Agricultural and Forest Meteorology* **46**: 193–209.
Schneiderman EM, Pierson DC, Lounsbury DG, Zion MS. 2002. Modeling the Hydrochemistry of the Cannonsville Watershed with Generalized Watershed Loading Functions (GWLF). *Journal of the American Water Resources Association* **38**(5): 1323–1347.
Schneiderman EM, Steenhuis TS, Thongs DJ, Easton ZM, Zion MS, Neal AL, Mendoza GF, Walter MT. 2007. Incorporating variable source area hydrology into the curve number based Generalized Watershed Loading Function model. *Hydrological Processes* **21**: 3420–3430.